First Results from SLD with Polarized Electron Beam at SLC*

The SLD Collaboration
Stanford Linear Accelerator Center
Stanford, CA 94309

represented by

Michael J. Fero
Massachusetts Institute of Technology
Cambridge, MA 02139

ABSTRACT

The SLAC Linear Collider (SLC) has been modified to collide a longitudinally polarized electron beam with the unpolarized positron beam. We review the beginning of polarized beam running at the SLC, and report on the measurement of the left-right cross section asymmetry (A_{LR}) made with a sample of 10,224 Z decays collected over the course of the 1992 run. The average beam polarization for this set of Z decays was $22.4 \pm 0.6\%$(syst.). A_{LR} was measured to be 0.100 ± 0.044(stat.)± 0.004(syst.). From this measurement, the weak mixing angle defined at the Z boson pole is determined to be $\sin^2 \theta_W^{\rm eff} = 0.2378 \pm 0.0056 \pm 0.0005$.

*Work supported by the Department of Energy, contract DE-AC03-76SF00515.

1. Introduction

The SLAC Linear Accelerator (SLC) began running with a polarized electron beam on April 19th, 1992. By May 2nd, the first Z bosons produced through collisions between the polarized electron beam and the unpolarized positron beam had been collected by the SLD detector. Since then, the SLD has collected over 11,000 Z events with polarized beam. With an average electron beam polarization of about 22%, the first measurement of the left-right cross section asymmetry (A_{LR}) has been performed. We report here on some aspects of polarized electron beam running at the SLC and present our measurement of A_{LR}.

The motivation for pursuing the left-right asymmetry at the SLC stems from its sensitivity to the electroweak mixing angle, and its insensitivity to systematic effects. Details about precision electroweak measurements, and the properties of A_{LR} in particular, have been described elsewhere [1—3]. We comment briefly on the physics motivating its measurement.

1.1 Physics Motivation for Measuring A_{LR}

The dynamics of the electroweak sector of the Standard Model are determined to lowest order by three parameters: the SU(2) coupling constant (g), the U(1) coupling constant (g'), and the vacuum expectation value of the Higgs field ($\langle\phi\rangle$). The values of these parameters can be extracted from a number of related experimental quantities, of which we list several in Table I. With the high precision mass measurements of the Z boson from LEP, the experimental quantities determining the Standard Model are taken to be: the electromagnetic fine structure constant (α), the fermi coupling constant (G_F), and the mass of the Z boson (M_Z).

Table I

Quantities Determining Standard Model Parameters			
Quantity	EW Parameter	Current Value	Precision (PPM)
α	$\frac{1}{4\pi}\frac{g^2 g'^2}{g^2+g'^2}$	$1/137.0359895(61)$	0.045
G_F	$\frac{\sqrt{2}}{2}\frac{1}{\langle\phi\rangle^2}$	$1.16639(2)\times 10^{-5}\,\mathrm{GeV}^2$	17
M_Z	$\frac{1}{2}\langle\phi\rangle\sqrt{g^2+g'^2}$	$91.187 \pm 0.007\,\mathrm{GeV}$	77
M_W	$\frac{\langle\phi\rangle g}{2}$	$80.22 \pm 0.26\,\mathrm{GeV}$	3241
$\sin^2\theta_W^{\mathrm{eff}}$	$\frac{g'^2}{g^2+g'^2}$	0.2324 ± 0.0011	4733

Additional measurements of EW observables beyond the first three listed would serve to over-constrain the model. However, the expressions given in the table relating M_Z, M_W, and $\sin^2\theta_W^{\mathrm{eff}}$, to g, g' and $\langle\phi\rangle$ are valid only to lowest order. Virtual electroweak corrections that depend (strongly) on the top quark mass (m_t) and (weakly) on the Higgs boson mass (m_H) must be included. Only within the uncertainties due to the lack of knowledge of m_t and m_H do the measurements of additional electroweak quantities serve to over-constrain the model, and thus test it. When the top quark mass is well measured, the tests will become stronger, and in fact, may place an upper limit on the Higgs boson mass.

We have listed two additional promising measurements: the measurement of the W boson mass (M_W), and a precision measurement of the weak mixing angle ($\sin^2\theta_W^{\mathrm{eff}}$). The mixing angle $\sin^2\theta_W^{\mathrm{eff}}$ is defined here in terms of the vector (v_f) and axial vector (a_f) couplings of the Z to fermion pairs via [4],

$$\begin{aligned} a_f &= T_f^3 \\ v_f &= T_f^3 - 2Q_f \sin^2\theta_W^{\mathrm{eff}} \quad , \end{aligned} \tag{1}$$

where T_f^3 is the third component of weak isospin for fermion f, and Q_f is the charge of the fermion.

At the SLC we pursue a precise determination of $\sin^2\theta_W^{\rm eff}$ via the measurement of the left-right asymmetry, which we now describe.

1.2 The Left-Right Asymmetry

The left-right asymmetry is defined as,

$$A_{LR} \equiv \frac{\sigma_L - \sigma_R}{\sigma_L + \sigma_R} \quad , \tag{2}$$

where σ_L and σ_R are the e^+e^- production cross sections for Z bosons (at the Z pole) with left-handed and right-handed electrons, respectively. To leading order, the Standard Model predicts that this quantity depends upon the vector (v_e) and axial-vector (a_e) couplings of the Z boson to the electron current,

$$A_{LR} = \frac{2v_e a_e}{v_e^2 + a_e^2} = \frac{2\left(1 - 4\sin^2\theta_W^{\rm eff}\right)}{1 + \left(1 - 4\sin^2\theta_W^{\rm eff}\right)^2} \quad . \tag{3}$$

In practice, we measure A_{LR} with a partially polarized electron beam, $\mathcal{P}_e = (N^+ - N^-)/(N^+ + N^-)$, where $N^{+(-)}$ is the number of beam electrons with spin parallel (anti-parallel) to the beam direction. In terms of the measured cross section asymmetry (A_m),

$$A_{LR} = \frac{A_m}{\mathcal{P}_e} \equiv \frac{1}{\mathcal{P}_e}\frac{N_L - N_R}{N_L + N_R} \quad , \tag{4}$$

where N_L and N_R are the number of Z bosons produced with left-and right-handed beam respectively. The error on the measurement of the weak mixing angle depends on the number of Z events and the error in the beam polarization measurement in the following way, where we take $\sin^2\theta_W^{\rm eff}$ such that $A_{LR} = 0.14$:

$$\delta\sin^2\theta_W^{\rm eff} = \frac{1}{7.9}\cdot\sqrt{A_{LR}^2\left(\frac{\delta\mathcal{P}_e}{\mathcal{P}_e}\right)^2 + \frac{1}{\mathcal{P}_e^2 N_Z}} \quad . \tag{5}$$

We can use the following argument to motivate Eq. (4):

1. In general, the lowest order diagrams for e^+e^- annihilation include direct photon exchange, direct Z exchange, and a $\gamma - Z$ interference term. However, the cross section formula is simple at the Z pole. At the pole the direct photon exchange term is small, and the $\gamma - Z$ interference term vanishes. The only part of the cross section that is significant is the Z exchange term.
2. The polarized electron beam will annihilate with positrons of the correct helicity in order to produce the (spin 1) Z polarized in the direction of the incident electron polarization.
3. The rate for Z production is

$$\sigma(\mathcal{P}_e) \sim N^- g_L^2 + N^+ g_R^2 \quad , \tag{6}$$

where N^+ is the number of electrons in the beam with positive helicity (spin pointing in the direction of beam propagation), and N^- is the number with negative helicity. $g^2_{L(R)} = v_e \pm a_e$ is the neutral current coupling of the left-(right) handed electron $e^-_{L(R)}$ and left-(right) handed positron $e^+_{L(R)}$ to the Z.

4. Reversing the beam polarization on a random basis ensures that equal amounts of data are taken with both senses of polarization, and that the luminosity is not tied to any periodic effects in the SLC. The asymmetry for Z production by the two polarization states is then given by,

$$\begin{aligned} A_m =& \frac{N(\mathcal{P}_e = L) - N(\mathcal{P}_e = R)}{N(\mathcal{P}_e = L) + N(\mathcal{P}_e = R)} \\ =& \frac{(N^- g_L^2 + N^+ g_R^2) - (N^+ g_L^2 + N^- g_R^2)}{(N^- g_L^2 + N^+ g_R^2) + (N^+ g_L^2 + N^- g_R^2)} \\ =& \left(\frac{N^+ - N^-}{N^+ + N^-}\right)\frac{g_L^2 - g_R^2}{g_L^2 + g_R^2} \\ =& \mathcal{P}_e \frac{2v_e a_e}{v_e^2 + a_e^2} \equiv \mathcal{P}_e A_{LR} \end{aligned} \tag{7}$$

The left-right asymmetry is only one of several measurements of the neutral current couplings to the Z being pursued. At LEP, the forward-backward asymmetries for b-quarks, muons and taus, as well as the tau polarization and its forward-backward asymmetry have been measured to moderate precision. All of these measurements are sensitive to the weak mixing angle, and in some cases (such as the forward-backward asymmetry for tau polarization) they measure exactly the same combination of coupling constants as A_{LR}. However, the A_{LR} measurement has properties which are particularly attractive for making a high precision measurement and deserve mention [2]:

1. A_{LR} is sensitive to the electroweak mixing parameter.
2. All of the visible final states except electron pairs can be used to measure A_{LR}.
3. A_{LR} does not depend on the final state couplings to the Z.
4. A_{LR} is independent of detector acceptance.
5. A_{LR} is independent of final state mass effects.
6. A_{LR} is insensitive to initial state radiation and is insensitive to small changes in $\sqrt{s}$.
7. QCD corrections vanish at the Z pole.
8. The theoretical uncertainty is small. It is dominated by the uncertainty on the renormalization of the electromagnetic coupling constant to the Z mass scale ($\delta A_{LR}(theory) \sim 0.002$).
9. The left-right asymmetry is sensitive to m_t and m_H via virtual electroweak radiative corrections.

The statistical and systematic advantages of A_{LR} over other techniques are of course very important if the SLD measurement is to compete with the LEP measurements of the electroweak asymmetries. We include in the concluding section of the paper a comparison of our results to those of LEP. We turn now to a discussion of polarization at SLC and the measurement of A_{LR}.

2. The Polarized SLC

The earliest references to a polarized SLC are found in a series of talks given by Charles Prescott in 1980 [10]. This early influence is seen in the design of the damping ring transfer lines, which accommodate the present spin transport scheme, as well as in the SLC polarized source technology, which is a direct descendant of the polarized source used for the E122 parity violation experiment performed at SLAC in 1977. Figure 1 shows a diagram of the SLC showing its polarization-related features. The important features of the polarized SLC are the polarized source, spin rotators before and after the damping rings, transfer lines to and from the damping rings, the SLC North Arc, and two polarimeters: the Møller polarimeter at the end of the linac, and the Compton polarimeter near the e^+e^- interaction point [5-9].

2.1 The Polarized Electron Source

Longitudinally polarized electrons are produced at the Polarized Electron Source by illuminating a GaAs photocathode with circularly polarized light from a laser of wavelength 715 nm. In GaAs, electrons pumped from the $P_{3/2}$ valence band into the $S_{1/2}$ conduction band, with right-handed circularly polarized light, are preferentially right-handed in a 3:1 ratio. This leads to a maximum theoretical polarization in such cathodes of 50%. A surface treatment of the GaAs with cesium and NF_3 provides a negative work function and high quantum efficiencies for the photoemission of conduction band electrons.

The SLC polarized source achieved remarkable success during the 1992 run. A fairly stable high current beam (6×10^{10} electrons per pulse) was produced off the surface of a bulk GaAs cathode with quantum efficiencies ranging from 3-10%. It was assumed that with sufficient laser power high electron currents off the cathode surface could be obtained up to the space charge limit of the gun. As it turns out, an additional charge limit comes into effect before the space charge limit and reduces the peak current that can be produced off the photocathode [11]. It was only

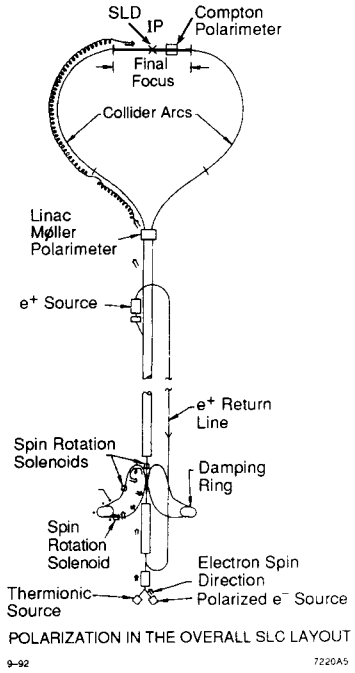

Fig. 1. The layout of the SLC emphasizing polarization. The orientation of the electron spin vector is shown by the double arrow.

by virtue of the very high quantum efficiencies that adequate source current was achieved. An important contribution to good gun performance was the cooling of the photocathode to just above 0°C. This provided an increase in cathode lifetime, reducing the frequency of interventions needed to re-treat the cathode with cesium to increase quantum efficiency. The polarized source operated quite efficiently, delivering beam to the SLC over 93% of the time.

2.2 The Spin Rotation System

Longitudinally polarized electrons produced at the source are accelerated to 1.16 GeV before injection into the damping ring. A system of three spin rotating solenoidal magnets, together with the fixed dipole magnets in the Linac to damping ring transfer lines, are used first to rotate the spin into the transverse plane of the damping ring, and then to orient the spin properly for transport down the linac and through the SLC arcs, so that the spin polarization is again longitudinal at the e^+e^- interaction point. The spin rotators are superconducting solenoidal magnets with field integrals between ±6.34 T-m.

The transport of polarized beams was accounted for in the design of the beam transport lines to and from the Linac to the damping ring. For electrons moving through a transverse magnetic field, both the momentum vector and the spin component perpendicular to the magnetic field rotate about an axis defined by the magnetic field direction. The degree of precession is related to the angle of bend by:

$$\theta_{spin} = \frac{g-2}{2}\gamma\theta_{bend} \quad .$$

The Linac to Ring (LTR) spin rotation system was designed to operate at the damping ring energy of 1.21 GeV. At this energy, the LTR transport line has the proper magnetic bend ($5 \times 32.8°$) to allow a full $5\pi/2$ rotation of the component of electron spin in the bend plane, while the Ring to Linac (RTL) line provides a $3\pi/2$ spin rotation. For technical reasons, the SLC damping rings were initially commissioned at 1.15 GeV. The energy was raised slightly, to 1.16 GeV, for the

polarized beam run. This implies a 19° deficit in the amount of spin rotation that the fixed magnets in the LTR can provide, and thus a 5% loss in polarization at the damping ring.

2.3 The Polarimeters

2.3.1 Linac Møller Polarimeter

At the end of the Linac an invasive measurement of the beam polarization is possible by means of a Møller polarimeter placed along the PEP extraction line. Figure 2 shows a diagram of the Linac Møller polarimeter. The polarimeter exploits the cross section asymmetry in the scattering of polarized 46 GeV beam electrons from polarized target electrons in thin magnetized iron foils. From 10-15 Møller electrons are scattered from the target foil for each 3×10^{10} electron beam pulse. A set of PEP extraction line magnets is used to momentum-analyze the Møller scatters, and electrons in the interval from 14-15 GeV/c are detected by a finely segmented silicon strip detector. The differential cross section for polarized Møller scattering is given by [3],

$$\frac{d\sigma_p}{d\theta} = \frac{d\sigma_u}{d\theta}\left[1 - \mathcal{P}_z^{beam}\mathcal{P}_z^{trgt}A_z(\theta) - \mathcal{P}_t^{beam}\mathcal{P}_t^{trgt}A_t(\theta,\phi)\right], \qquad (8)$$

where σ_p is the polarized cross section, θ is the cm frame scattering angle, σ_u is the unpolarized Møller scattering cross section, $\mathcal{P}_z^{beam}$ and $\mathcal{P}_z^{trgt}$ are the longitudinal polarizations of the beam and target, $\mathcal{P}_t^{beam}$ and $\mathcal{P}_t^{trgt}$ are the transverse polarizations of the beam and target, and $A_z(\theta)$ and $A_t(\theta,\phi)$ are the longitudinal and transverse asymmetry functions.

The beam polarizations are extracted using the asymmetry formed by reversing the sign of either the target or beam polarization and measuring the counting rates,

$$\mathcal{P}_z^{beam} = \frac{1}{\mathcal{P}_z^{trgt}A_z}\cdot\left[\frac{R(\mathcal{P}_z^{trgt}\mathcal{P}_z^{beam}>0) - R(\mathcal{P}_z^{trgt}\mathcal{P}_z^{beam}<0)}{R(\mathcal{P}_z^{trgt}\mathcal{P}_z^{beam}>0) + R(\mathcal{P}_z^{trgt}\mathcal{P}_z^{beam}<0)}\right] = \frac{A_{M\text{ø}ller}^{measured}}{\mathcal{P}_z^{trgt}A_z}. \qquad (9)$$

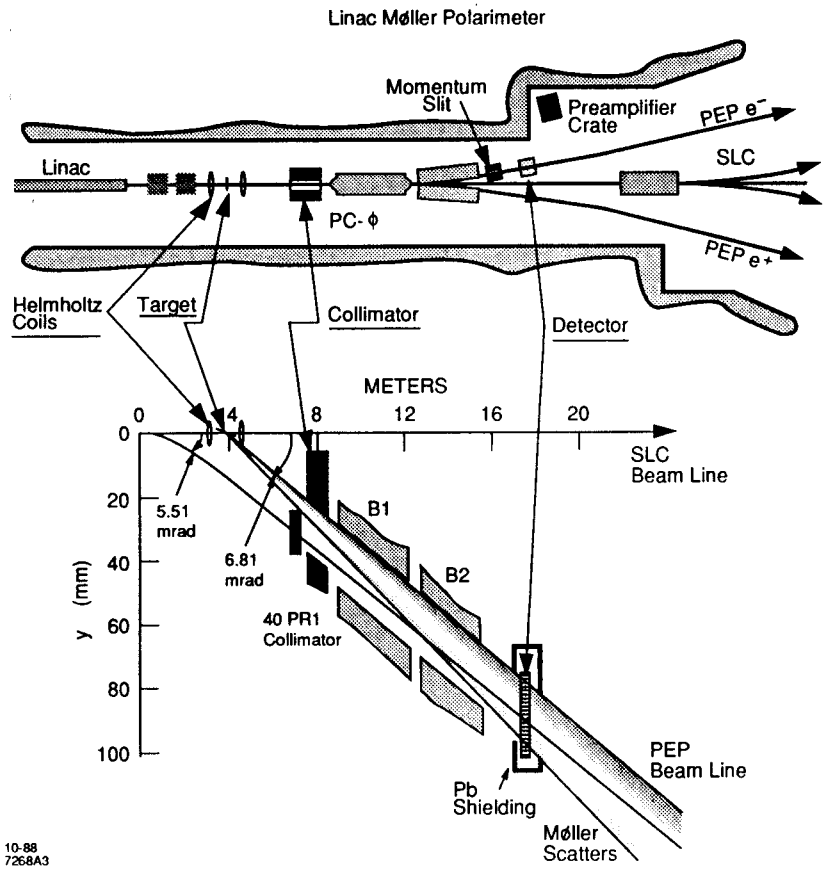

Fig. 2. The layout of the Linac Møller Polarimeter.

For most of the Møller polarimeter running, a thin, 50.8 μm (2 mils), target foil was used. Inclined at an angle of 20° with respect to the beam, the target foil presents an effective thickness of 152 μm (6 mils) to the electron beam. The target foil polarization measurement dominates the Møller polarimeter systematic error. The measured target foil polarization was 7.97 $\pm$ 0.26% for the 2 mil foil.

At nominal beam currents, the Møller polarimeter was able to measure longitudinal polarizations with a statistical error of 1% in approximately 30 minutes. Results using the Møller polarimeter will be given in the section on beam depolarization.

2.3.2 Compton Polarimeter

The Compton polarimeter is used for continuous measurement of the beam polarization near the e^+e^- interaction point. The polarimeter is based on Compton scattering of the electron beam off circularly polarized photons. Figure 3 shows a diagram of the polarimeter. The outgoing 45.7 GeV electron beam collides with a 2.33 eV circularly polarized photon beam at a γe^- collision point 33 m downstream from the SLC e^+e^- interaction point. Since the electron scattering angles are smaller than the angular divergence of the incident beam, the scattered and unscattered beams remain unseparated until they pass through a pair of SLC dipole magnets of field integral 3.05 T-m. The scattered electrons are dispersed horizontally and exit the vacuum system through a thin window. Electrons in the energy interval 17-30 GeV are detected and their momentum analyzed by a pair of multichannel detectors located 3.57 m and 3.87 m downstream of the effective bend center of the dipole pair.

The differential cross section for the Compton scattering of longitudinally polarized electrons and circularly polarized photons is given by [12],

$$\frac{d\sigma_p}{dE_s} = \frac{d\sigma_u}{dE_s}\left[1 + \mathcal{P}_\gamma \mathcal{P}_e A\left(E_s\right)\right], \tag{10}$$

where σ_p is the polarized cross section, E_s is the energy of the scattered electron,

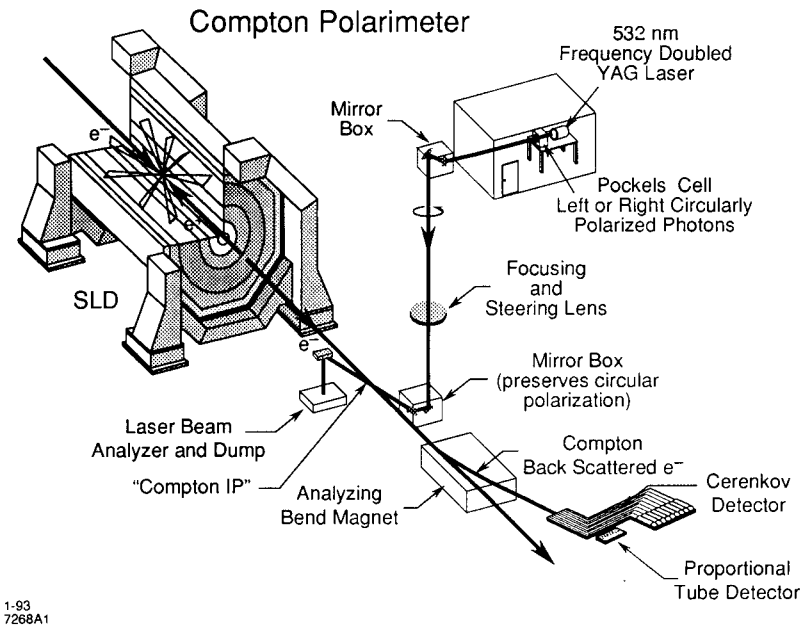

Fig. 3. A diagram of the Compton Polarimeter.

σ_u is the unpolarized Compton scattering cross section, $\mathcal{P}_\gamma$ is the photon spin polarization in the helicity basis [13], $\mathcal{P}_e$ is the longitudinal polarization of the electron, and $A(E_s)$ is the Compton asymmetry. The unpolarized cross section and the asymmetry function depend upon the energies of the electron and photon beams. The largest cross section and asymmetry occur at the kinematic limit $E_s = 17.4$ GeV, corresponding to a scattering angle of 180 degrees in the electron rest frame. The asymmetry is zero at $E_s = 25.2$ GeV and becomes negative for larger energies. We measure the counting rates in the detectors for anti-parallel and parallel combinations of beam helicities, $R(\mathcal{P}_\gamma\mathcal{P}_e > 0)$ and $R(\mathcal{P}_\gamma\mathcal{P}_e < 0)$, respectively. It follows from Eq. (10) that the asymmetry formed from these rates determines the electron beam polarization,

$$\mathcal{P}_e = \frac{1}{\mathcal{P}_\gamma \langle A \rangle} \cdot \left[\frac{R(\mathcal{P}_\gamma\mathcal{P}_e > 0) - R(\mathcal{P}_\gamma\mathcal{P}_e < 0)}{R(\mathcal{P}_\gamma\mathcal{P}_e > 0) + R(\mathcal{P}_\gamma\mathcal{P}_e < 0)}\right] = \frac{A^{meas}_{Compton}}{\mathcal{P}_\gamma \langle A \rangle}, \qquad (11)$$

where $\langle A \rangle$ is the average Compton asymmetry for the energy interval subtended by the detector channel used to measure the rate asymmetry.

2.4 First Polarized Beam to the SLD: a Lesson in Spin Transport

The leading electron pulse for SLC is accelerated in the Linac to 46.7 GeV before the beam enters the North Arc of the machine. As it traverses the North Arc, the electron bunch trajectory undergoes a total bend of 236 degrees, while the component spin in the transverse plane precesses through approximately 70 complete rotations. The spin vector in the Linac is set with the two spin rotating solenoids after the damping ring, in order to accommodate spin precession in the arc, while maximizing the longitudinal component of spin at the e^+e^- interaction point. It was decided that for the first polarized beam in SLC, only the LTR and RTL spin rotators would be used. This enabled a somewhat simpler initial setup of the SLC. Spin transport studies had shown that for this configuration, the absolute value of the longitudinal spin vector at the interaction point would be almost at a maximum at the beam energy corresponding to the Z peak, and should thus be easily observable with the Compton polarimeter. As it happened, the first measurements of the longitudinal component of the electron beam polarization near the e^+e^- interaction point were very close to zero. A quick scan of the beam polarization as a function of beam energy revealed that a significant degree of polarization was in fact present (see Fig. 4). The longitudinal component of the beam polarization as a function of beam energy is a cosine-like function as expected, but the phase and period are shifted from those predicted by the spin transport simulation.

An empirical procedure was employed, this time using both the RTL and the Linac spin rotators, to maximize the longitudinal spin component at the e^+e^- interaction point. The procedure involves measuring the longitudinal component of the beam polarization near the e^+e^- interaction point with the Compton polarimeter for each of the three orthogonal spin directions at the end of the Linac. The measured components can then be used to predict the proper spin rotator settings needed to achieve a fully longitudinal beam at the e^+e^- interaction point at a given energy, and, when added in quadrature, the measurements give the full beam polarization available in the machine.

After the first test of this procedure, a scan of the polarization with respect to beam energy showed the polarization peaking near the Z peak beam energy as intended (see Fig. 4).

This early running showed that the SLC North Arc had an unexpected influence on spin direction at the e^+e^- interaction point. The betatron advance of an SLC achromat (there are 23 achromats in an SLC arc) is 1085°, while the spin precession through one of these achromats is 1080°. Depending on the relative phases of spin and betatron oscillation, either the initial horizontal or longitudinal spin component will couple into the vertical. Even though the effect is small in each achromat, the cumulative effect can be large. A dramatic indication of this coupling is shown in polarization data taken while varying the launch of the electron beam into the SLC arc. As shown in Fig. 5, small changes in the launch

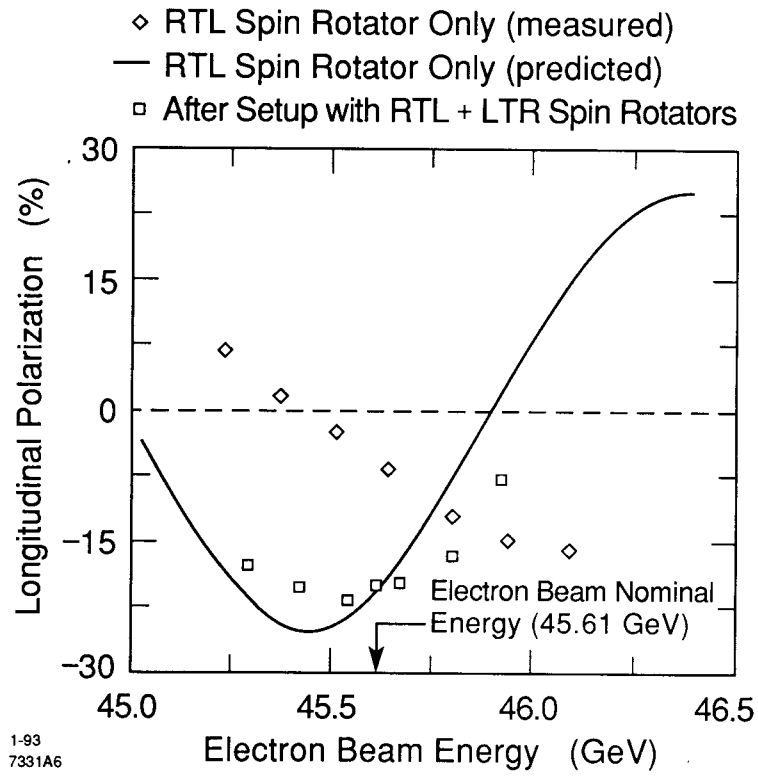

Fig. 4. The first measurements of longitudinal beam polarization near the e^+e^- interaction point as a function of beam energy. Using the RTL spin rotator only, the beam polarization did not peak at the expected energy. Using a combination of RTL and Linac spin rotators, the longitudinal polarization at the e^+e^- interaction point can be maximized.

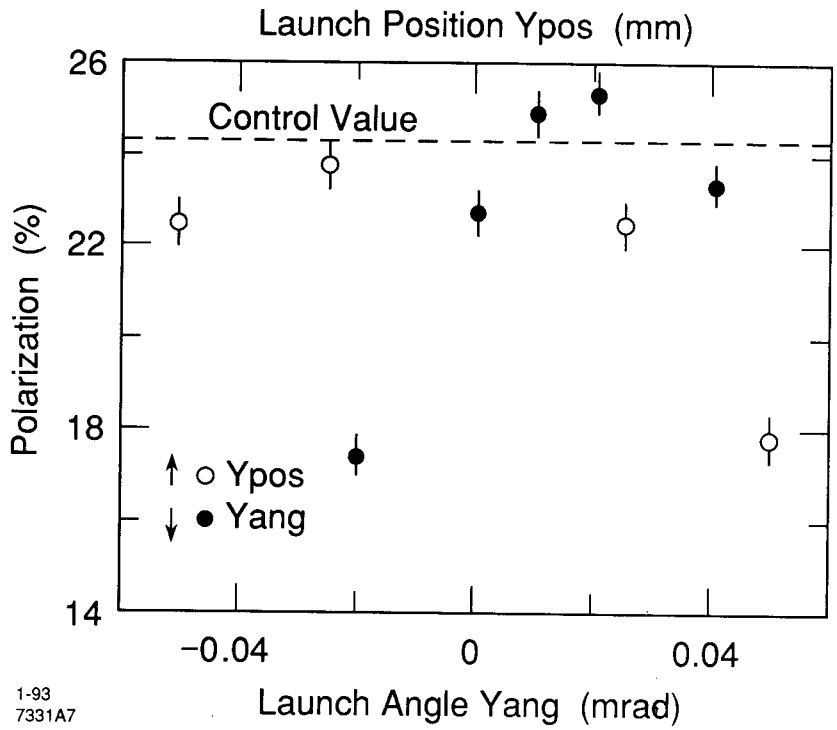

Fig. 5. A scan of SLC launch angle and position show the strong effect on the degree of longitudinal polarization observed near the e^+e^- interaction point.

position or angle cause substantial changes in the way the spin precesses in the North Arc, and thus, in the degree of longitudinal polarization seen near the e^+e^- interaction point. Since the phenomenon was noticed, more detailed spin transport studies have shown that betatron oscillations of the order of 25 microns are sufficient to cause significant spin rotation in the arcs [14]. Changes in arc orbit are gradual and easily monitored with the Compton polarimeter. Figure 6 shows the time history of polarization measured for each Z detected by SLD. The majority of the width of the distribution is attributed to polarization drift due to changing machine conditions.

2.5 Beam Depolarization

The amount of beam depolarization from source to IP can be checked with measurements made by the two polarimeters. The Linac Møller Polarimeter measurements were made with both straight-ahead beam bypassing the damping rings, and also with beam through the damping ring. Most of the Linac Møller data was taken with damped beam. In this configuration, the unit polarization vector had components $\hat{p}_x = -0.56$, $\hat{p}_y = 0.277$, and $\hat{p}_z = 0.781$ in the Linac.

From the 1992 Møller data it was found that:

1. $P_z = 27.1 \pm 0.8\%(\text{stat.}) \pm 1.5\%(\text{syst.})$, as measured for beam that goes directly from the source to the Møller polarimeter at the end of the Linac, is consistent with measurements of $P_z = 28 \pm 1\%(\text{syst.})$ made in the lab using a Mott scattering polarimeter and the same type of bulk GaAs source and a laser wavelength of 715 nm [15].
2. $P_z = 25.9 \pm 1.0\%(\text{stat.}) \pm 1.5\%(\text{syst.})$ for beam that stays in the damping ring for one machine cycle (8.3 ms). The ratio between the longitudinal spin polarization for damped vs. undamped beam is 0.956 ± 0.05, which is consistent with a factor of 0.95 for the spin transmission of the damping ring, and a factor of 0.97 for the fact that the RTL can not fully rotate the spin into the longitudinal direction at 1.16 GeV.

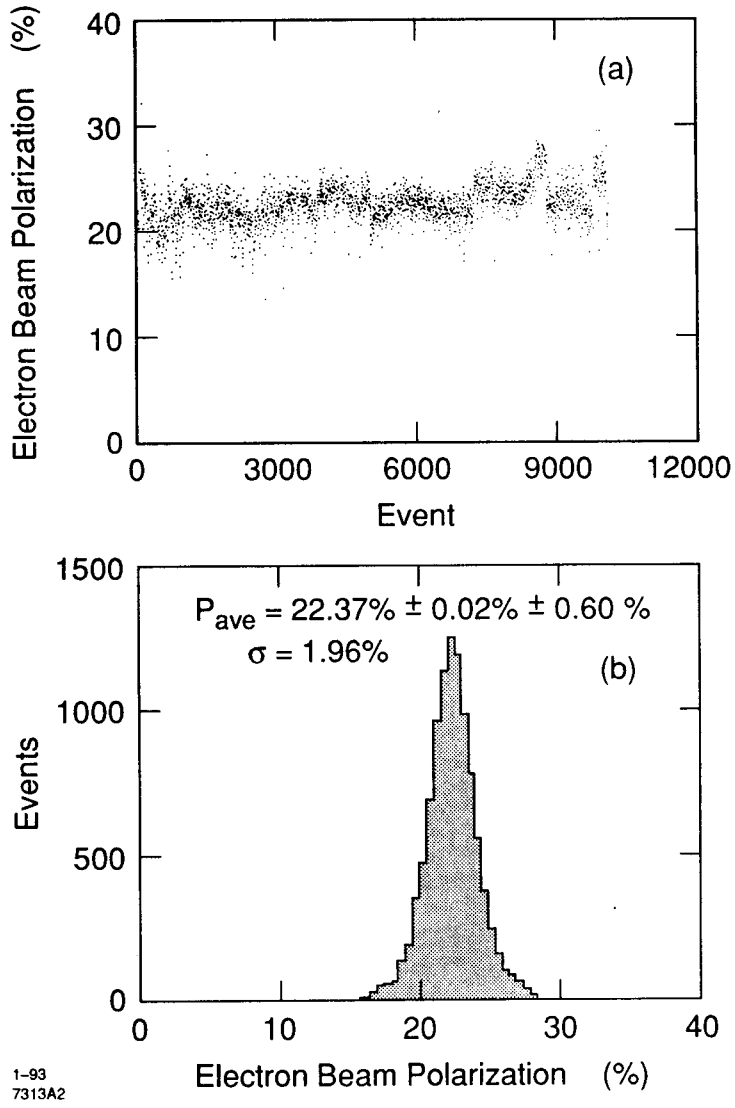

Fig. 6. Beam polarization measurements for each Z selected by the SLD detector.

If we assume a source polarization of 28%, we expect that the maximum polarization observable near the e^+e^- interaction point should be about 25.3%. We have assumed a 0.95 spin transmission through the damping ring due to the LTR energy mismatch, and another 0.95 spin transmission in the North Arc due to the beam energy spread.

Compton Polarimeter measurements averaged over the bulk of the run showed an average beam polarization of 22.4%. This final factor of 0.88 is due to the vagaries of the SLC North Arc orbit. Indeed, on several occasions high polarization (over 25%) was measured near the e^+e^- interaction point. Unfortunately, the machine state that lead to the highest polarizations was difficult to characterize, and stable running at the highest polarizations was not achieved. It is of interest, for future running at the SLC, that the spin dynamics of the North Arc be understood, at least empirically, so that the maximum longitudinal polarization can be delivered to the interaction point.

3. Measuring the Left-Right Asymmetry

We measure A_{LR} by counting hadronic and $\tau^+\tau^-$ decays of the Z boson for each of the two longitudinal polarization states of the electron beam. The measurement requires knowledge of the absolute beam polarization, but does not require knowledge of the absolute luminosity, detector acceptance, or efficiency [16].

3.0.1 Polarization Measurements

The beam polarization is related to the measured Compton asymmetry ($A^{meas}_{Compton}$), the photon beam polarization ($\mathcal{P}_\gamma$), and the polarimeter analyzing power ($\langle A \rangle$) by

$$\mathcal{P}_e = \frac{A^{meas}_{Compton}}{\mathcal{P}_\gamma \langle A \rangle}. \tag{12}$$

Any channel in either of the two electron detectors with large analyzing power can be used to measure the beam polarization, assuming that the analyzing power for that channel is well understood. The beam polarization measurements, thus far, have been made with the two highest analyzing power (sixth and seventh) channels of the Cherenkov detector. The sixth and seventh channels detect electrons in the energy intervals 18.4-19.6 GeV and 17.3-18.4 GeV, respectively. The average Compton scattering asymmetries (analyzing powers) for these intervals are 0.6154 and 0.7027, respectively. The channel-by-channel polarization asymmetry as measured by the Cherenkov detector is shown in Fig. 7. The mean electron energy E for each channel includes a small correction for showering in the pre-radiator and channel walls. The detector position and spectrometer momentum scale are determined from measurements of the minimum electron energy point and the zero-asymmetry point. The theoretical asymmetry function $A(E_s)$ is shown as a continuous line in the figure, with absolute normalization adjusted to provide the best fit to the data [17].

Limits have been placed on systematic effects such as the linearity of the phototube/ADC detection system, stability of the calibration, electronic cross talk, and biases in the measurement of the background. The total systematic error arising from these sources is estimated to be 1.8% [17]. The laser beam polarization was monitored continuously throughout the run and was measured directly at the Compton interaction point both before and after the run. A plane polarizer was rotated in the beam and maximum and minimum transmitted intensities recorded with a photodiode. The circular polarization is calculated using $\mathcal{P}_\gamma = 2\sqrt{I_{min}I_{max}}/(I_{min}+I_{max})$. From the direct measurements and the spread in monitored photon polarization values, we measure a photon polarization of 93±2%. A determination of the absolute electron beam helicity was made by exploiting the known cross section difference between the J=1/2 and J=3/2 γe^- interactions [18].

The total systematic error on the measurement is estimated to be $\delta\mathcal{P}_e/\mathcal{P}_e = 2.7\%$, dominated by the error on the laser beam polarization at the Compton interaction point. The systematic uncertainties that affect the polarization measurement are summarized in Table II [19].

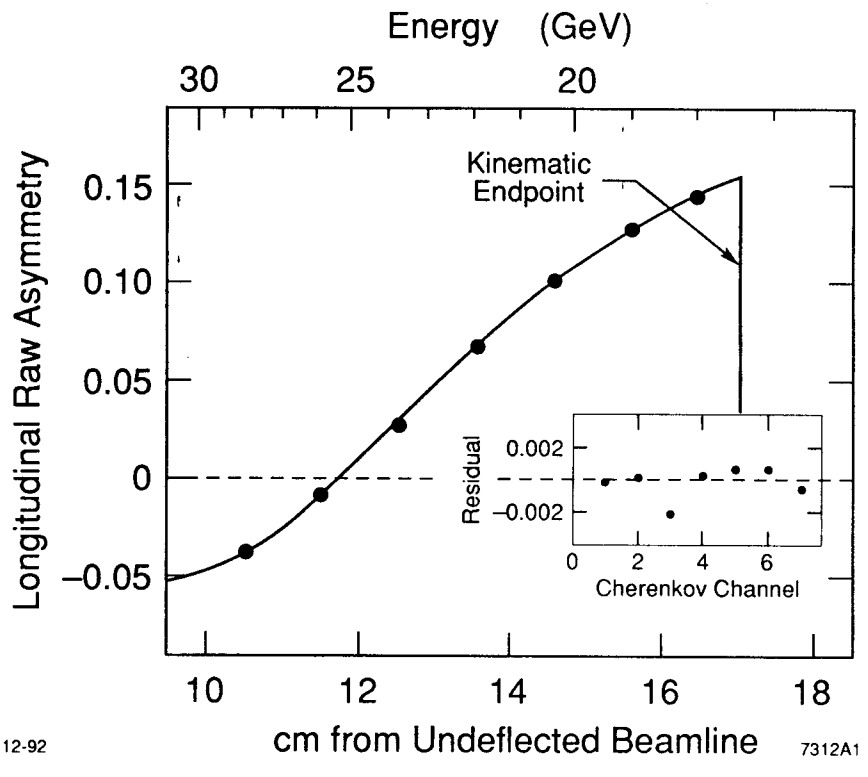

Fig. 7. The polarization asymmetry measured by seven channels of the Cherenkov detector. The solid line represents the best fit of the theoretical asymmetry function to the data.

Table II

Polarization Measurement Systematic Uncertainties	
Laser Polarization	2%
Spectrometer Calibration	0.4%
Detector Linearity	1.5%
Interchannel Consistency	0.9%
Electronic Noise Correction	0.4%
Total	2.7%

We have performed a number of checks of the polarization measurement. The polarimeter measures the electron scattering rate for two helicity states each of electrons and photons. We therefore measure two independent nonzero asymmetries and two independent null asymmetries. We verified that the nonzero asymmetries are consistent, and that the null asymmetries are consistent with zero.

An additional systematic error would arise if the average beam polarization at the electron-photon crossing point differed from the luminosity-weighted average beam polarization at the e^+e^- interaction point. We have investigated phase space and beam transport effects, depolarization caused by beam-beam interactions at the interaction point [20], and an effect caused by the possible systematic deviation of the luminosity-weighted mean beam energy from the average beam energy [21]. All of these effects cause fractional polarization differences that are smaller than 0.1%.

The polarimeter provides a beam polarization measurement every few minutes. The time history of polarization measurements associated with Z events is shown in Fig. 6. The average beam polarization for this set of Z data is $22.4 \pm 0.6\%$(syst.).

3.1 Z Event Selection

The e^+e^- collisions are measured by the SLD detector [22]. For this measurement, the triggering of the SLD and the selection of Z events were based solely on calorimetry.

The Liquid Argon Calorimeter (LAC) [23], which covers 98% of the full solid angle, is segmented in depth into two electromagnetic (21 X_0 total) and two hadronic (2.8 λ for the entire LAC) sections, each of which is transversely segmented into projective towers of constant solid angle (there are a total of $\sim 17,000$ towers in the first electromagnetic section).

The calorimetric analysis must distinguish Z events from several backgrounds that are unique to the operation of a linear collider. The backgrounds fall into two major categories: those due to low-energy electrons and photons that scatter from various beam line elements and apertures, and those due to high-energy muons that traverse the detector parallel to the beam axis (due to the low average current in the SLC, backgrounds caused by beam collisions with residual gas in the beam line are negligible). The beam-related backgrounds in the calorimeters are characterized by small amounts of energy in a large number of towers parallel to the beam. In order to suppress these backgrounds, all towers used in the analysis are required to satisfy a combination of threshold cuts and criteria that select against longitudinally localized energy deposition in a combined electromagnetic-hadronic tower. Each candidate event must contain fewer than 3000 accepted towers (of the 40,000 total), and the total energy observed in the endcap region of the Warm Iron Calorimeter (WIC) [24] where beam backgrounds are large, must be less than 12 GeV. All events are required to satisfy a set of selection criteria based on total visible energy (at least 20 GeV in the LAC) and energy balance.

We estimate that the combined efficiency of the trigger and selection criteria is (90±2)% for hadronic Z decays and about 30% for tau pairs. Because the event selection is calorimeter based, muon pairs are not included in our sample. We compare this selection procedure with one based on tracking information, and a Monte Carlo simulation. From these studies, we estimate that the residual beam-related background in the Z sample is less than 0.7%. The contribution of two-photon processes to the Z sample has been estimated by a Monte Carlo simulation to be less than 0.1%. Final state e^+e^- events are explicitly removed, since the presence of the t-channel photon exchange subprocess dilutes the value of A_{LR}. We apply an e^+e^- identification procedure which searches for large and highly localized energy deposition in the electromagnetic section of the LAC. The residual e^+e^- background in the Z sample is approximately 0.7%.

The sign of the electron beam helicity is supplied to the SLD data acquisition system via two redundant data paths. The synchronization of the helicity signals with triggered and logged events was verified on several occasions.

3.2 Results

A total of 10,224 Z events satisfy the selection criteria. We find that 5,226 of the events were produced with the left-handed electron beam and 4,998 were produced with the right-handed beam.

The measured left-right cross section asymmetry for Z production is

$$A_m = (5226 - 4998)/10224 = (2.23 \pm 0.99) \times 10^{-2},$$

where the error is statistical only. The measured asymmetry is related to A_{LR} by the following expression which is accurate to first order in the correction terms:

$$A_{LR} = \frac{A_m}{\mathcal{P}_e} \cdot + \frac{1}{\mathcal{P}_e}\left[A_m f_b + A_m^2 A_{\mathcal{P}} - E\frac{\sigma'(E)}{\sigma(E)}A_E - A_\varepsilon - A_{\mathcal{L}}\right], \qquad (13)$$

where $\mathcal{P}_e$ is the luminosity-weighted average beam polarization, f_b is the background fraction, $\sigma(E)$ is the unpolarized Z cross section at center-of-mass energy E, $\sigma'(E)$ is the derivative of the cross section with respect to E, and $A_{\mathcal{P}}$, A_E, A_ε, and $A_{\mathcal{L}}$ are respectively the left-right asymmetries of the beam polarization, the

center-of-mass energy, the product of detector acceptance and efficiency, and the integrated luminosity [25]. The correction to A_m for background contamination is less than 3.1×10^{-4}. The polarization asymmetry is directly measured to be $A_{\mathcal{P}} = -2.9 \times 10^{-3}$, resulting in a negligible correction. A left-right beam current asymmetry would give rise to a left-right energy asymmetry via beam-loading of the accelerator. Using the measured left-right current asymmetry, we infer that the A_E correction to A_m is $(1.7\pm0.6)\times10^{-5}$. The SLD has a symmetric acceptance in polar angle [16] which implies that the efficiency asymmetry A_ε is negligible.

A significant left-right luminosity asymmetry could be produced only by an asymmetry of the beams emitted by the polarized electron source. Such effects are expected to be quite small [8]. We verify this by examining a sample of 25,615 small-angle Bhabha scattering events selected with the LUM system. Of these, 12,832 events were produced with the left-handed electron beam and 12,783 were produced with the right-handed beam. Since the left-right cross section asymmetry for small-angle Bhabha scattering is expected to be small ($\sim3\times10^{-4}\cdot\mathcal{P}_e$ in the acceptance of the LUM detector), the left-right asymmetry formed from the luminosity Bhabha events is a direct measure of $A_{\mathcal{L}}$. We measure $A_{\mathcal{L}}$ to be $(1.9\pm6.2)\times10^{-3}$. A more precise determination of $A_{\mathcal{L}}$ follows from a study of the three parameters of the electron beam (all defined at the interaction point) that determine the SLC luminosity: the beam current, the electron-positron beam offset, and the beam size (the beam is approximately round). The first two quantities are measured directly. Beam size is not measured directly but can be inferred from the flux of beamstrahlung photons produced by beam-beam interactions at the interaction point. By measuring the left-right asymmetries of each of these quantities, we conclude that $A_{\mathcal{L}}$ is $(1.8\pm4.2)\times10^{-4}$.

Since all corrections listed in Eq. (13) are consistent with zero or are extremely small, we do not apply them to A_m, but include them in the systematic uncertainty on A_{LR}.

The luminosity-weighted average polarization is estimated, from measurements of the beam polarization made when valid Z events are recorded, to be:

$$\mathcal{P}_e = \frac{1}{N_Z}\sum_{i=1}^{N_Z}\mathcal{P}_i = (22.4 \pm 0.7)\%, \tag{14}$$

where N_Z is the total number of Z events and $\mathcal{P}_i$ is the polarization measurement associated in time with the i^{th} event. The error on $\mathcal{P}_e$ is dominated by the systematic uncertainty on the polarization measurement. We find the left-right asymmetry to be

$$A_{LR} = \frac{A_m}{\mathcal{P}_e}0.100 \pm 0.044(\text{stat.}) \pm 0.004(\text{syst.}).$$

The systematic error is dominated by the error of the polarization determination, but contains contributions from the uncertainties in f_b and $A_{\mathcal{L}}$ (see Table III).

Table III

A_{LR} Systematic Uncertainties	
Polarization Uncertainty	2.7%
Luminosity Asymmetry	1.9%
Background Fraction	1.4%
Total	3.6%

We use this measurement to derive the following value for the effective electroweak mixing parameter [26]:

$$\sin^2\theta_W^{\text{eff}} = 0.2378 \pm 0.0056(\text{stat.}) \pm 0.0005(\text{syst.}),$$

where we have corrected the result to account for the deviation of the SLC center-of-mass energy from the Z-pole energy and for initial state radiation [27]. These results are consistent with recent measurements of τ polarization and the leptonic forward-backward asymmetries made by the LEP experiments [28—31]. A comparison with some recent LEP measurements is shown in Fig. 8.

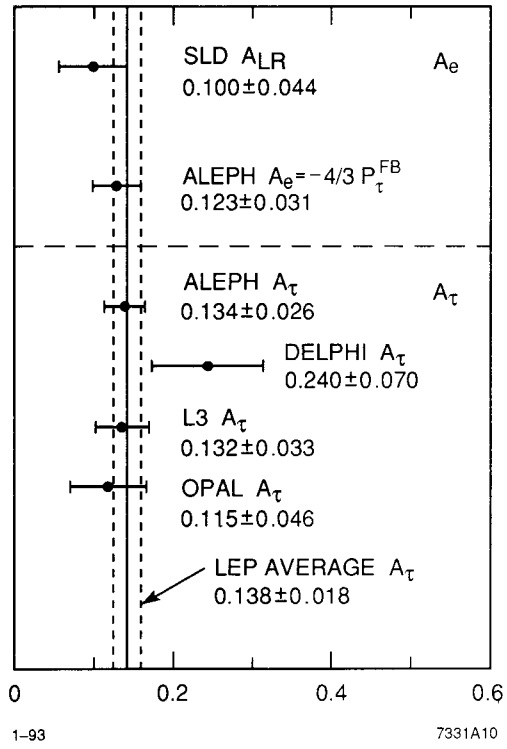

Fig. 8. A comparison of our recent measurement of A_{LR} to comparable LEP electroweak measurements.

4. Conclusions

The success of the first SLD physics run was highlighted by the first running of polarized beam in the SLC. By exploiting the polarized beam at SLC, we have demonstrated the use of a new, statistically powerful, and systematically precise technique for testing the Standard Model.

The most dramatic indication of the strength of the method is seen in the comparison with recent LEP results shown in Fig. 8. With a comparatively small number of events, 10^4 for SLD vs. 10^6 per LEP experiment, we are already able to make a competitive measurement of the weak mixing angle. Futhermore, with the anticipated rise in beam polarization and luminosity in 1993 (polarization greater than 40%, 40-60 thousand Z bosons), we expect to make a high precision measurement of $\sin^2\theta_W^{\rm eff}$ in the near future. Figure 9 shows the expected error on $\sin^2\theta_W^{\rm eff}$ as a function of the integrated number of Z bosons in our event sample. With our present average beam polarization, measurements of $\sin^2\theta_W^{\rm eff}$ with errors ~ 0.001 are possible only with a fairly substantial increase in machine luminosity. As the figure shows, the situation improves dramatically with higher beam polarization.

If new high polarization strained lattice cathodes [32] can be made to deliver full beam current at the proper wavelength, we can anticipate 80% polarization at the source, as opposed to the 28% seen in 1992. With this degree of longitudinal beam polarization, a $\delta\sin^2\theta_W^{\rm eff} \leq 0.001$ measurement is possible with the 50,000 Z bosons expected in 1993 [33].

Acknowledgements

We would like to thank the personnel of the SLAC Accelerator Department and the technical staffs of our collaborating institutions for their outstanding efforts on our behalf. The author would also like to thank Morris Swartz and Peter Rowson for substantial portions of the text of this document, and the members of the SLD Electroweak working group for their helpful comments and suggestions.

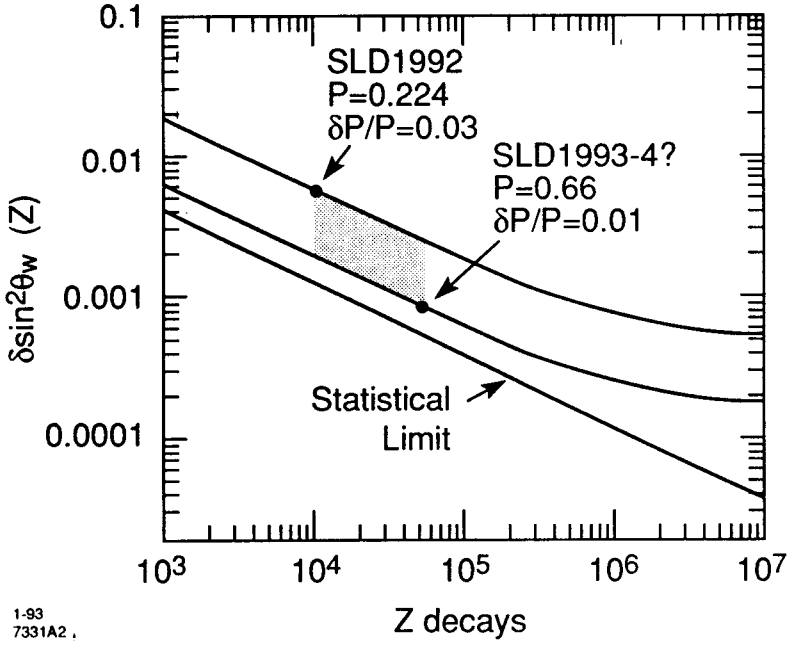

Fig. 9. The expected error on $\sin^2\theta_W^{\rm eff}$ as a function of the integrated number of Z bosons in our event sample. Curves are shown for beam polarization as measured in 1992, and for future high polarization.

REFERENCES

1. A review of the properties of A_{LR} can be found in D.C. Kennedy *et al.*, *Nuc. Phys.* **B321**, 83 (1989).
2. A good descriptive account of precision electroweak measurements is found in M. L. Swartz *Precision Experiments in Electroweak Interactions*, SLAC-PUB-5219, March 1990.
3. A detailed description of polarization at SLC and physics with polarized beams is found in M. L. Swartz *Physics with Polarized Beams*, SLAC-PUB-4656, June 1988.
4. We follow the convention used by the LEP Collaborations in *Phys. Lett.* **B276**, 247 (1992).
5. D. Blockus *et al.*, Proposal for Polarization at the SLC, April 1986.
6. N. Phinney, Review of SLC Performance, SLAC-PUB-5864, August 1992.
7. D. Schultz *et al.*, *The Polarized Electron Gun for the SLC*, SLAC-PUB-5768, March 1992.
8. M. Woods *et al.*, *Polarized Light Sources for the SLC*, SLAC-PUB-5965, December 1992.
9. M. Fero *et al.*, *The Compton Polarimeter for SLC*, SLAC-PUB-6026, December 1992.
10. C. Y. Prescott, Prospects for Polarized Electrons at High Energies, *XVII International School of Subnuclear Physics, Erice, Italy, July 31 - Aug. 11, 1980*, SLAC–PUB–2630, October 1980, and C. Y. Prescott, Polarized e^+e^- Physics in Linear Colliders, *The 1980 Int. Symp. on High Energy Physics with Polarized Beams and Targets, Lausanne, Switzerland, Sept. 25 - Oct. 1, 1980*, SLAC–PUB–2649, November 1980.
11. M. Woods *et al.*, SLAC-PUB-5894, September 1992.

12. H. A. Olsen, *Applications of QED*, Springer Tracts in Modern Physics, Vol. 44, p.83, (1968); S. B. Gunst and L. A. Page, *Phys. Rev.* **92**, 970 (1953); F. W. Lipps and H. A. Tolhoek, *Physica* **20**, 395 (1954).

13. Note that the high energy physics convention based on the photon spin differs by a sign from the convention used in optics. A photon with left-handed circular polarization has right-handed helicity, $P_\gamma = +1$.

14. T. Fieguth and M. Petrazda, private communication.

15. T. Maruyama, R. Prepost, private communication.

16. The value of A_{LR} is unaffected by decay-mode-dependent variations in detector acceptance and efficiency provided that the efficiency for detecting a fermion at some polar angle is equal to the efficiency for detecting an antifermion at the same polar angle. The SLD has an azimuthally symmetric solenoidal magnetic field and a high degree of uniformity and polar symmetry, which ensures the equality of particle and antiparticle efficiencies.

17. B. Schumm and R. Elia, SLD Note 222, November 1992.

18. M. Fero *et al.*, SLD Note 221, October 1992, and references therein.

19. This error should drop below 1% in the next run with the installation of new laser beamline hardware. In particular, we now measure over 99% circular polarization at the Compton interaction point since realigning the beam line and replacing a mirror pair that was not well compensated.

20. K. Yokoya and P. Chen, SLAC-PUB-4692, September 1988.

21. See J. Kent *et al.*, SLAC-PUB-4922, March 1989, and G.S. Abrams *et al.*, *Phys. Rev. Lett.*, **63**, 2173 (1989).

22. The SLD Design Report, SLAC Report 273, May 1984.

23. D. Axen *et al.*, SLAC-PUB-5354, January 1990 (to be published in Nuclear Instruments and Methods).

24. A.C. Benvenuti *et al.*, SLAC-PUB-5713, January 1992.

25. P. C. Rowson, *et al.*, SLD Note 176, April 1990.

26. The result given here supersedes the result presented at the summer school of $A_{LR} = 0.02 \pm 0.07 \pm 0.001$, which was based on $\sim 5K$ events. The new number is the result of improved statistics and the correction of an over sign error in the Compton polarimeter analysis.

27. The correction from the result given by Eq. 4 is +0.0003. Our calculation agrees with the results given by the EXPOSTAR program described in D.C. Kennedy *et al.*, *Z. fur Phys.*, **C53**, p. 617, 1992, and a modified version of the ZSHAPE program described in CERN 89-08, vol. 3, p. 50, 1989.

28. ALEPH Collaboration: D. Decamp *et al.*, *Z. Phys.* **C53**, 1 (1991) and *Phys. Lett.* **B265**, 430 (1991).

29. DELPHI Collaboration: P. Aarnio *et al.*, *Nucl. Phys.* **B367**, 511 (1992) and P. Abreu *et al.*, *Z. Phys.* **C55**, 555 (1992).

30. L3 Collaboration: B. Adeva *et al.*, *Z. Phys.* **C51**, 179 (1991) and O. Adriani *et al.*, *Phys. Lett.* **B294**, 466 (1992).

31. OPAL Collaboration: G. Alexander *et al.*, *Z. Phys.* **C52**, 175 (1991) and *Phys. Lett.* **B266**, 201 (1991).

32. T. Maruyama *et al.*, SLAC-PUB-6033, December 1992.

33. If the damping rings are run at 1.19 GeV, the polarization loss in the linac-to-damping ring transfer line will be reduced to only 0.7%. Assuming no other improvements in reducing spin transport losses we can expect an average beam polarization throughput of $\sim$ 83%. This implies roughly 66% polarization at the e^+e^- interaction point given a source polarization of 80%.